Three-body losses of a polarized Fermi gas near a *p*-wave Feshbach resonance in effective field theory

M. Schmidt [1], H.-W. Hammer [1,2] and L. Platter [3,4,*]

[1]*Technische Universität Darmstadt, Department of Physics, 64289 Darmstadt, Germany*
[2]*ExtreMe Matter Institute EMMI, GSI Helmholtzzentrum für Schwerionenforschung GmbH, 64291 Darmstadt, Germany*
[3]*Department of Physics and Astronomy, University of Tennessee, Knoxville, Tennessee 37996, USA*
[4]*Physics Division, Oak Ridge National Laboratory, Oak Ridge, Tennessee 37831, USA*

We study three-body recombination of fully spin-polarized ^{6}Li atoms that are interacting resonantly in relative *p* waves. Motivated by a recent experiment, we focus on negative scattering volumes where three atoms recombine into a deep dimer and another atom. We calculate the three-body recombination rate using a Faddeev equation derived from effective field theory. In particular, we study the magnetic field and temperature dependences of the loss rate and use the recombination data to determine the effective range of the *p*-wave atom-atom interaction. We also predict the existence of a shallow three-body resonance state that manifests itself as a prominent feature in the energy-dependent three-body recombination rate.

I. INTRODUCTION

Experiments with ultracold atomic gases provide a unique way to explore the interactions between atoms. Specifically, strongly interacting system have recently received a lot of attention [1–5]. For example, the loss rate of an ultracold system of strongly interacting bosons will display discrete scale invariance when it is measured as a function of the scattering length. This discrete scale invariance is related to the well-known Efimov effect [6] and displays a log-periodic dependence of the three-body loss rate on the scattering length [7–10]. Three-body losses occur in ultracold atomic gases as a result of three-body collisions in which the atoms gain kinetic energy due to the formation of a two-body bound state. Indeed, the Efimov effect was first observed through its signature in three-body losses in a cold gas of Cs atoms [11].

Identical fermions cannot interact in a relative *s* wave due to the Pauli principle. However, their *p*-wave scattering volume can be tuned, and a number of experiments have examined the features of strongly interacting Fermi gases [12–17]. The Efimov effect does not occur in these systems [18–20]; however, losses still occur through recombination processes into shallow or deep dimers. The three-body losses in spin-polarized ultracold gases of ^{6}Li were recently studied in the group of Takashi Mukaiyama at Osaka University, focusing on scaling laws [15], unitary-limited behavior [16], and the role of cascade processes [17].

In this paper, we focus on the data taken by Waseem *et al.* [16]. Specifically, they considered the $|F = 1/2, m_F = +1/2\rangle$ hyperfine state and measured the loss rate at large negative *p*-wave scattering volume, enhanced by a Feshbach resonance at $B_0 = 159.17(5)$ G.

At negative scattering volume, three atoms recombine into a so-called deep dimer, i.e., a dimer whose binding energy is so large that it cannot be described by the parameters of the effective range expansion. The authors of this work used a simplified Breit-Wigner model for the energy-dependent three-body recombination rate $K_3(E)$ to determine information about the atom-atom interaction and to model the temperature-dependent three-body loss rate $L_3(T)$. While they managed to reproduce the measured loss data appropriately, we will discuss in detail that their simplified approach also has some important limitations.

It is particularly important to have an accurate microscopic description for the three-body recombination if the goal is to extract two-body observables from three-body processes with some understanding of the resulting uncertainties. Various approaches can be used to develop a microscopic description of this process. Effective field theory (EFT) uses the separation between short- and long-range scales in a system to construct a controlled expansion. It has been applied successfully in particle, nuclear, and atomic physics [1,21,22]. The parameters that appear in the EFT description of atomic systems with strong interactions can be related directly to the effective range parameters. This approach is therefore model independent and facilitates an unbiased analysis of experimental data. Systems with *p*-wave interactions were previously studied using the short-range effective field theory [20]. It was found that a real three-body parameter is required for renormalization. However, the emphasis of that work was on renormalization issues and the spectrum of three-body states.

Here, we will use EFT to study the three-body loss rate for recombination into deep dimers at finite temperature with the parameters relevant to the experimental measurements by Waseem *et al.* [16]. We will construct the interaction of two atoms in a relative *p* wave and use it to derive a Faddeev equation for the three-body system. Its solution allows us to

———
[*]Corresponding author: lplatter@utk.edu

compute the three-body recombination rate $K_3(E)$. Temperature averaging then yields the three-body loss rate $L_3(T)$. Comparison with the data obtained by Waseem *et al.* will let us draw conclusions about the features of the two-body interaction such as the *p*-wave effective range. Moreover, it will allow us to tie these features to other three-body observables such as the energy of a shallow three-body resonance state.

In this study, we restrict ourselves to a leading-order description of the loss rate within an EFT valid in the nonunitary regime, i.e., at energies below the two-body resonance where a single partial wave dominates. The EFT expansion discussed below allows us to estimate higher-order corrections in terms of typical momentum scales, yielding theory uncertainty bands for the loss rate. These bands also indicate the beginning of the unitary regime where the EFT breaks down since formerly higher-order terms become significant. Thus, a different power counting would have to be developed for the unitary regime. However, that is beyond the scope of this paper.

This paper is organized as follows. In Secs. II and III, we introduce our microscopic framework to calculate the three-body loss rate. Some details of the EFT framework are given in the appendixes. Our results are presented and compared to the data by Waseem *et al.* [16] in Sec. IV. We end with a short summary and outlook in Sec. V.

II. RECOMBINATION NEAR A *p*-WAVE RESONANCE

At sufficiently low energies, the elastic scattering properties of particles can be quantified using the effective range expansion. In the *p* wave, the expansion is

$$k^3 \cot \delta_1 = -\frac{1}{a_1} + \frac{r_1}{2}k^2 + \cdots, \qquad (1)$$

where δ_1 is the scattering phase shift, a_1 denotes the scattering volume, r_1 is the effective range, and the ellipses denote higher-order terms. We note that our definition of the effective range r_1 differs by a factor of -2 from the definition used in Ref. [16]. For a van der Waals interaction, the expansion $k^3 \cot \delta_1$ in powers of the momentum k contains a term linear in k. However, it was shown first by Levy and Keller [23] and later by Gao [24] using quantum defect theory for the van der Waals interaction and by Zhang *et al.* [25] in a two-channel Feshbach resonance model that this term is proportional to a_1^{-2}. Zhang *et al.* proposed to use the ratio of $1/a_1$ and the linear term at the relevant momentum scale to quantify its importance. We find that this ratio is maximally 2×10^{-7} for the thermal momenta and scattering volumes considered in this work. We will therefore ignore this term in the following discussion.

The level scheme of three spin-polarized ^{6}Li atoms in the hyperfine state $|F = 1/2, m_F = +1/2\rangle$ is illustrated in Fig. 1. Two identical ^{6}Li atoms form a deeply bound state denoted ^{6}Li$_2$(d). The Feshbach resonance creates an excited state ^{6}Li$_2$(e), whose position can be tuned by changing the magnetic field B. The scattering volume of two ^{6}Li atoms in the $|F = 1/2, m_F = +1/2\rangle$ state, a_1, diverges at the resonance position, $B_0 = 159.17(5)$ G. For $B \approx B_0$, the magnetic
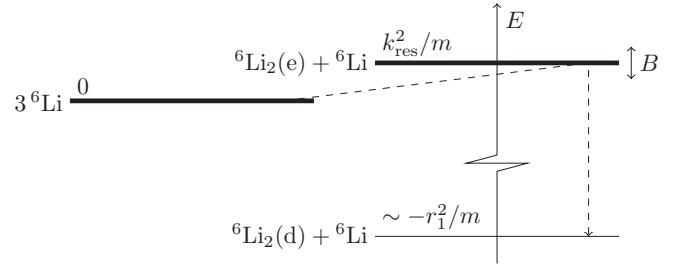

FIG. 1. Level scheme of three spin-polarized ^{6}Li atoms in the hyperfine state $|F = 1/2, m_F = +1/2\rangle$. Three-body recombination into a deeply bound state ^{6}Li$_2$(d) proceeds through the Feshbach resonance state ^{6}Li$_2$(e). Its position $k_{\text{res}}^2(B)/m$ can be tuned by a magnetic field B.

field dependence has the form

$$a_1(B) = a_{1,\text{bg}}\left(1 + \frac{\Delta B}{B - B_0}\right) \approx \frac{a_{1,\text{bg}} \Delta B}{B - B_0}, \qquad (2)$$

where $a_{1,\text{bg}} < 0$ is the background scattering volume and $\Delta B > 0$ is the resonance width [16].[1] As input, we use the value $a_{1,\text{bg}} \Delta B = -2.8(3) \times 10^6 a_B^3$ G, obtained in a fit to the thermalization rate of the spin-polarized ^{6}Li gas by Nakasuji *et al.* [26]. For fixed $B \approx B_0$, $a_1(B)$ is then given with an uncertainty of roughly 10%.

The *p*-wave effective range r_1 is usually assumed to depend weakly on B in the immediate vicinity of B_0 [16,26,27]. Waseem *et al.* suggested the near-resonance estimate

$$(r_1)_{\text{est}} \equiv \frac{2}{m \, \delta\mu \, a_{1,\text{bg}} \Delta B} = -0.182(20) \, a_B^{-1} \qquad (3)$$

and used it in their analysis of the experimental data [16]. In Eq. (3), $\delta\mu = 113(7)k_B \, \mu\text{K G}^{-1}$ denotes the relative magnetic moment between ^{6}Li$_2$(e) and two ^{6}Li atoms, with k_B being Boltzmann's constant. We adopt the assumption that r_1 is constant in B. However, we note that different estimates for r_1 have been given that differ significantly from $(r_1)_{\text{est}}$. First, Bruun *et al.* derived Eq. (3) only for two bosons near an *s*-wave Feshbach resonance [28]. Second, Nakasuji *et al.* obtained a different value $-0.116(10)a_B^{-1}$ in their fit to the thermalization rate [26]. They also cited an even smaller theory prediction, $-0.096(6)a_B^{-1}$, by Julienne (Ref. [29] of their work). This value deviates by roughly 50% from Eq. (3). Thus, r_1 introduces the largest uncertainty to the study. It is one goal of this work to predict r_1 from data of the three-body loss rate L_3.

In the experiment by Waseem *et al.*, recombination was studied for $B - B_0 > 0$ ($a_1 < 0$), where the process can be distinguished from background losses [16]. Thus, we restrict ourselves to this region when calculating L_3. On this side of the Feshbach resonance, the two-body system has a resonance pole above threshold representing the ^{6}Li$_2$(e) state.[2] The position of the corresponding maximum of the scattering

---

[1]For detunings $B - B_0 < 0.5$ G as in [16], the constant term in Eq. (2) is less than 1% of the total and can be neglected.

[2]For $B - B_0 < 0$ (corresponding to $a_1 > 0$), ^{6}Li$_2$(e) is a shallow bound state.

amplitude on the real k axis will be denoted by k_{res} (see Fig. 1). It varies with B and will be denoted "resonance momentum" in the following. For a large scattering volume, the resonance momentum can be approximated by [29,30]

$$k_{\mathrm{res}}(B) = \sqrt{\frac{2}{a_1(B)r_1}}. \tag{4}$$

Note that $k_{\mathrm{res}}(B)$ is real valued since both $a_1(B)$ and r_1 are negative for the Feshbach resonance considered in this paper.

The Feshbach resonance introduces a strong separation of momentum scales to the two-body system. In particular, the resonance momentum $k_{\mathrm{res}}(B)$ is much smaller than the natural (high) momentum scale set by the effective range r_1. Such a separation is an important requirement for the EFT approach. In the system at hand, it enables an expansion of the two-body scattering amplitude in terms of the ratio $\chi_2(B) \equiv k_{\mathrm{res}}(B)/r_1 \ll 1$. This expansion yields a simple Breit-Wigner-like diatom propagator at leading order in the expansion in $\chi_2(B)$ [30]. In the following, we restrict our analysis to leading order (LO) in the expansion in $\chi_2(B)$.

For $B - B_0 > 0$, three-body recombination proceeds in the absence of a shallow dimer state only into deep dimer states $^6\mathrm{Li}_2(d) + {}^6\mathrm{Li}$. Such a process involves a large excess of kinetic energy $\sim r_1{}^2/m$ outside our EFT's applicability region; that is, the recombination process happens when all three atoms are very close together. While the process cannot be described in detail in the framework of our EFT, the total rate for recombination into deep dimers can be described by making the three-body parameter complex [31]. This corresponds to using an optical three-body potential to model the losses at short distances which can be treated in perturbation theory [10].

As shown by Esry *et al.*, the recombination rate of three identical fermions vanishes at total kinetic energy $E = 0$ [32]. More specifically, it obeys the threshold law $K_3 \propto E^2$ in the partial-wave channel $J^P = 1^+$ and is suppressed by further powers of E for other J^P. Thus, we focus on the 1^+ channel at LO. To calculate the recombination rate K_3, the absolute square of the matrix element for the recombination process in the $J^P = 1^+$ channel, $\mathcal{M}^{1m_J}$ ($m_J \in \{-1, 0, 1\}$), has to be integrated over incoming momenta $\boldsymbol{p}_1$, $\boldsymbol{p}_2$, $\boldsymbol{p}_3$, summed over m_J, and divided by the three-body phase space ϕ_3, i.e.,

$$
\begin{aligned}
K_3(p_E) = {} & \frac{1}{\phi_3(p_E)} \left(\prod_{i=1}^{3} \int \frac{d^3 p_i}{(2\pi)^3} \right) (2\pi)^4 \, \delta^{(3)}\left(\sum_{i=1}^{3} \boldsymbol{p}_i \right) \\
& \times \delta\left(\frac{p_E^2}{m} - \sum_{i=1}^{3} \frac{p_i^2}{2m} \right) \\
& \times \sum_{m_J} \left| i\mathcal{M}^{1m_J}(\{\boldsymbol{p}_i\}; p_E) \right|^2,
\end{aligned} \tag{5}
$$

where $p_E^2/m \equiv E$. Explicit expressions for $\mathcal{M}$ and ϕ_3 will be given in Sec. III [see Eqs. (12) and (14)]. Equation (5) can then partially be evaluated analytically by integrating over the δ functions, as will be discussed below.

Data for three-body recombination are available only at finite temperature $T \sim \mu\mathrm{K}$ [16]. For this reason, we have to calculate the thermal average of K_3. The energy E is distributed

according to the Boltzmann distribution of three equal-mass particles which is proportional to $E^2 \exp[-E/(k_\mathrm{B}T)]$ (see, e.g., Refs. [33,34]). In terms of p_E, it follows that

$$\langle K_3 \rangle(T) = \frac{1}{(m\,k_\mathrm{B}T)^3} \int_0^\infty dp_E \; p_E^5 \, e^{-p_E^2/(m\,k_\mathrm{B}T)} K_3(p_E). \tag{6}$$

The thermal average is directly proportional to the experimentally measured loss rate [8,16]

$$L_3(T) = \tfrac{3}{6} \langle K_3 \rangle(T). \tag{7}$$

We reiterate that our focus is on three-body recombination into deep dimers. However, the same formalism can be used to study recombination into shallow dimers, i.e., three-body recombination for a positive two-body scattering volume a_1. A preliminary study of this case can be found in Ref. [30].

III. THREE-BODY RECOMBINATION MATRIX ELEMENT

In order to calculate the matrix element $\mathcal{M}^{1m_J}$ in Eq. (5), we require the atom-diatom scattering amplitude $T^{(1^+)}$ in off-shell kinematics. This amplitude can be obtained by solving an integral equation derived from effective field theory. In general, the total angular momentum $\boldsymbol{J} = \boldsymbol{l} + \boldsymbol{L}$ is the sum of the atom-atom orbital angular momentum $\boldsymbol{l}$ ($l = 1$) and the diatom-atom orbital angular momentum $\boldsymbol{L}$, implying $P = (-1)^{1+L}$. Thus, at small energies, the leading partial-wave channel $J^P = 1^+$ is given by the single combination $l = L = J = 1$. We restrict ourselves to this channel at LO. The theoretical uncertainty introduced by this approximation will be addressed at the end of this section. The partial-wave projected Faddeev integral equation for the amplitude $T^{(1^+)}$ reads [30]

$$
\begin{aligned}
T^{(1^+)}&(p, p'; p_E) \\
&= -V^{(1^+)}(p, p'; p_E) + \int_0^\Lambda \frac{dq\, q^2}{2\pi^2} V^{(1^+)}(p, q; p_E) \\
&\quad \times G_\pi\!\left(\tilde{k}(q^2)\right) T^{(1^+)}(q, p'; p_E),
\end{aligned} \tag{8}
$$

where

$$\tilde{k}(q^2) = i\sqrt{-p_E^2 + \frac{3}{4}q^2 - i\epsilon} \tag{9}$$

is a momentum variable and G_π is the Breit-Wigner-like LO diatom propagator

$$iG_\pi(\tilde{k}) = i\left[-a_1^{-1}(B) + \frac{r_1}{2}\tilde{k}^2 - ik_{\mathrm{res}}^3(B)\,\theta(B - B_0) \right]^{-1}, \tag{10}$$

which contains information on the two-body effective range parameters. Moreover, p (p') denotes the incoming (outgoing) atom-diatom relative momentum, and $p_E \equiv i(-mE - i\epsilon)^{1/2}$ is the momentum scale set by the total kinetic energy. The quantity

$$
\begin{aligned}
V^{(1^+)}(p, q; p_E) = {} & 8\pi[Q_0 - Q_2]\left(\frac{p_E^2 - p^2 - q^2}{pq} \right) \\
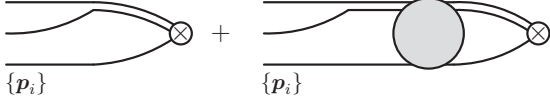& + \frac{H^{(1^+)}(\Lambda)pq}{\Lambda^2}
\end{aligned} \tag{11}
$$

FIG. 2. Matrix element for three-body recombination into a deeply bound state. The cross indicates the pointlike vertex for recombination into the deep dimer. The gray blob denotes the atom-diatom amplitude $T^{(1^+)}$ which is the solution of Eq. (8).

is the exchange potential arising from partial-wave projection of the single-atom exchange contribution, where Q_0 and Q_2 are Legendre functions of the second kind in the convention of Ref. [35]. The Faddeev equation (8) is equipped with a momentum cutoff of natural order, $\Lambda \sim r_1$ or larger, which also appears in the three-body force term. The three-body

force $H^{(1^+)}(\Lambda)$ is required for renormalization of the atom-dimer amplitude [20] and depends on the cutoff Λ. Details of the derivation, including the Feynman rules and partial-wave projection, can be found in Appendixes A and B. Note that for $B > B_0$, the diatom is unstable and does not represent an asymptotic state. However, the quantity $T^{(1^+)}(p, p'; p_E)$ is required in off-shell kinematics to calculate the three-body recombination matrix element $\mathcal{M}^{1m_J}$.

The three-body recombination matrix element $\mathcal{M}^{1m_J}$, depicted in Fig. 2, depends on the three incoming atom momenta $\boldsymbol{p}_i$ ($i \in \{1, 2, 3\}$). For identical fermions, the matrix element must be antisymmetric under exchange of each pair of momenta $\boldsymbol{p}_i, \boldsymbol{p}_j$ ($i \neq j$). This property is automatically taken care of by the anticommutation relations of the atom field operators $\psi, \psi^\dagger$ introduced in Appendix A. Applying the Feynman rules dictated by the effective Lagrangian of Eq. (A2) in Appendix A to the two diagrams in Fig. 2, we find

$$i\mathcal{M}^{1m_J}(\{\boldsymbol{p}_i\}; p_E) = iF^{(1^+)}(\Lambda) \, 3 \sqrt{\frac{2\pi}{m}} \sum_{\pi \in \mathcal{C}_3} \{\boldsymbol{p}_{\pi(1)} - \boldsymbol{p}_{\pi(2)}\}_{1m_l} G_\pi\big(\tilde{k}(p_{\pi(3)}^2)\big)$$

$$\times \left(C_{1m_L, 1m_l}^{1m_J} \{\boldsymbol{p}_{\pi(3)}\}_{1m_L} - \int \frac{d^3 q}{(2\pi)^3} T^{m_l, m_l'}(\boldsymbol{p}_{\pi(3)}, \boldsymbol{q}; p_E) G_\pi\big(\tilde{k}(q^2)\big) C_{1m_L, 1m_l'}^{1m_J} \{\boldsymbol{q}\}_{1m_L} \right), \tag{12}$$

where $C_{Lm_L, lm_l'}^{Jm_J}$ is a Clebsch-Gordan coefficient that couples the angular momenta $\boldsymbol{l}$ and $\boldsymbol{L}$ to $\boldsymbol{J}$ and the sum is over all even permutations π of (1 2 3), denoted $\mathcal{C}_3$. Sums over m_l, m_l', and m_L are implicit. The coefficient of the pointlike vertex for recombination into the deep p-wave dimer is given by $F^{(1^+)}(\Lambda)$. This regulator-dependent constant acts as a short-range optical potential. The general equation for the unprojected amplitude $T^{m_l, m_l'}$ in Eq. (12) including all partial waves is given in Appendix B. At LO, it reduces to its 1^+ component, i.e.,

$$T^{m_l, m_l'}(\boldsymbol{p}, \boldsymbol{q}; p_E) = T^{(1^+)}(p, q; p_E) \, 4\pi \sum_{m_J} \big[\boldsymbol{Y}_{(1,1)1m_J}(\hat{\boldsymbol{p}})\big]^{m_l} \big[\boldsymbol{Y}_{(1,1)1m_J}(\hat{\boldsymbol{q}})\big]^{m_l'*} \tag{13}$$

in the convention of Eq. (B2b). The tensor structure $\{\cdot\}_{1m}$ in Eq. (12) is defined in Eq. (A3).

To evaluate the expression for the recombination rate in Eq. (5), we further need the three-body phase space

$$\phi_3(p_E) = \frac{m \, p_E^4}{24\sqrt{3} \, \pi^2}. \tag{14}$$

Inserting Eqs. (12) and (14) and integrating over the δ functions, we obtain

$$K_3(p_E) = \frac{|F^{(1^+)}(\Lambda)|^2}{m} \frac{432\sqrt{3}}{p_E^4} \int_0^{\frac{2}{\sqrt{3}} p_E} dp_A \, p_A \int_0^{\frac{2}{\sqrt{3}} p_E} dp_B \, p_B \, \theta(1 - |x_0|)$$

$$\times \big[|p_A J(p_B; p_E)|^2 + 2 \operatorname{Re}\{p_B J(p_A; p_E)[p_A J(p_B; p_E)]^*\} \big], \tag{15}$$

where

$$x_0 \equiv \frac{1}{p_A p_B}\big(p_E^2 - p_A^2 - p_B^2\big), \tag{16a}$$

$$J(p; p_E) \equiv G_\pi\big(\tilde{k}(p^2)\big)\left(p - \int_0^\Lambda \frac{dq \, q^2}{2\pi^2} T^{(1^+)}(p, q; p_E) G_\pi\big(\tilde{k}(q^2)\big) q\right). \tag{16b}$$

The integral contained in the definition in J diverges as $\Lambda \to \infty$. This cutoff dependence is absorbed by an appropriate running of the short-range factor $|F^{(1^+)}(\Lambda)|^2$ with Λ. The running of $F^{(1^+)}$ can be obtained by making the three-body force $H^{(1^+)}$ in Eq. (11) required to renormalize $T^{(1^+)}$ complex. Thus, the running of $F^{(1^+)}$ with the cutoff Λ is

fully determined by the running of $H^{(1^+)}$. A similar procedure was previously used to describe three-body recombination into deep s-wave dimers [10].

Before we go on, we expand on the expected size of omitted partial waves compared to $J^P = 1^+$. For sufficiently small energies, their contributions to the recombination rate involve
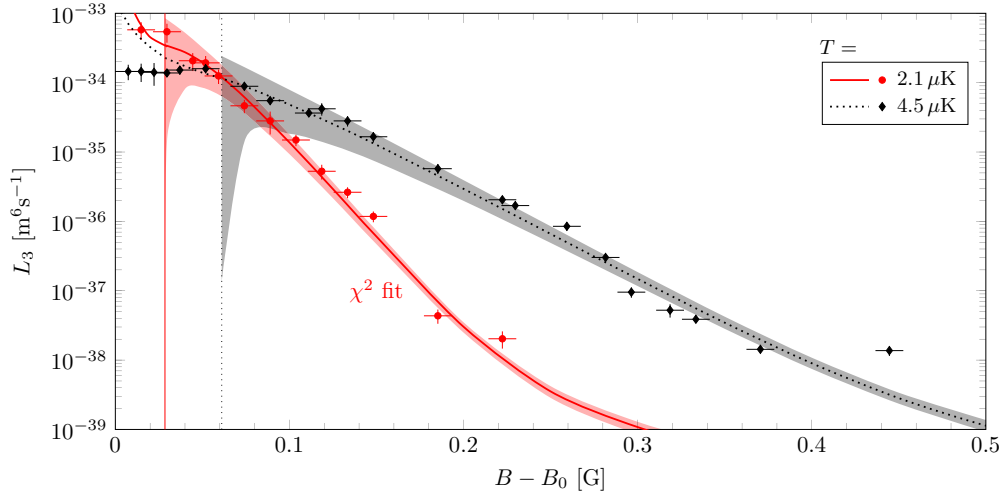
FIG. 3. Loss rate L_3 as a function of the field detuning $B - B_0$ for two temperatures T at $\Lambda = 0.4a_B^{-1}$. Vertical grid lines mark points at which $k_{\rm res}(B) = p_T$. They separate the unitary regime (left) from the nonunitary regime (right). The solid red curve is a χ^2 fit in $(r_1, H^{(1^+)}, F^{(1^+)})$ to the $T = 2.1\,\mu{\rm K}$ data in the nonunitary regime for $a_{1,\rm bg}\,\Delta B = -2.8 \times 10^6 a_B^3$ G. The black dotted curve is the resulting prediction for $T = 4.5\,\mu{\rm K}$. Uncertainty bands in the nonunitary regime follow from NLO corrections of the order of $p_T^2/k_{\rm res}^2(B) < 1$ and from the experimental uncertainty of $a_{1,\rm bg}\,\Delta B$. Naive application of the theory to the unitary regime leads to an overestimation of the data.

at least one more factor E [32]. Naively, one would compare this factor to the breakdown scale r_1^2/m set by the p-wave effective range. For $p_E \lesssim k_{\rm res}(B) = \chi_2(B)r_1$, that would yield an *a priori* uncertainty $p_E^2/r_1^2 \lesssim \chi_2^2(B)$ which is very small ($\lesssim 0.01\%$ for $B - B_0 \leqslant 0.5\,{\rm G}$). In obtaining this estimate, we have used the threshold laws of Ref. [32]. The work of Suno *et al.*, however, suggests that the threshold laws fail at $p_E = k_{\rm res}(B)$ [36]. At this point, formerly subleading channels may become comparable to $J^P = 1^+$. As a consequence, we apply our LO framework only to the low-energy region $p_E < k_{\rm res}(B)$. The *a priori* LO uncertainty at fixed energy can then be written as $\chi_3(B, E) \equiv p_E^2/k_{\rm res}^2(B) < 1$.

To estimate the LO uncertainty $\tilde{\chi}_3(B, T)$ at finite temperature, we set p_E to the maximum of the Boltzmann weighting factor in Eq. (6), i.e., to

$$p_T \equiv \sqrt{\frac{5}{2}mk_{\rm B}T}. \tag{17}$$

This yields the expression

$$\tilde{\chi}_3(B, T) \equiv p_T^2/k_{\rm res}^2(B) \approx \frac{r_1}{2}\,a_{1,\rm bg}\,\Delta B\,\frac{5}{2}mk_{\rm B}\,\frac{T}{B - B_0}, \tag{18}$$

where Eqs. (2) and (4) have been used. Note that we aim to determine r_1 from the data and thus do not use the approximate relation (3).

IV. RESULTS

A. Fit of free parameters and comparison with experiment

The data obtained in Ref. [16] can be divided into two different regimes, the unitary regime and the nonunitary regime. We define the unitary regime as the temperature domain in which the resonance momentum $k_{\rm res}$ is smaller than the thermal momentum scale p_T defined in Eq. (17). For a given resonance momentum $k_{\rm res}$, the unitary regime sets in at

temperatures larger than

$$T_{\rm unitary} = \frac{2k_{\rm res}^2}{5mk_{\rm B}}. \tag{19}$$

We do not expect our EFT to work in this regime since the expansion parameter $\tilde{\chi}_3(B, T) \gtrsim 1$. For convenience, we will drop the superscript 1^+ in the three-body terms H and F from now on.

We use our approach to fit the effective range r_1, the three-body force H, and the short-distance three-body parameter F to the experimental data for $T = 2.1\,\mu{\rm K}$ from Ref. [16]. Our results are renormalization group invariant and independent of Λ, but for definiteness we use an ultraviolet cutoff $\Lambda = 0.4a_B^{-1}$ in the integral equations. We find an effective range $r_1 = -0.11(2)a_B^{-1}$, which has the same order of magnitude as the result by Waseem *et al.* but deviates by 40%. The negative sign is consistent with the resonance momentum $k_{\rm res}(B)$ being real valued [see Eq. (4)]. For the three-body force, we find $H = 4^{+5}_{-7}$, and for the short-distance three-body parameter we obtain $\log_{10}(F/m^2) = 49.8^{+0.2}_{-0.1}$. We emphasize that these two quantities are not observables and depend on the ultraviolet cutoff Λ used to solve Eq. (8).

The red solid line in Fig. 3 shows the fitted loss rate L_3 in comparison to the experimental data (red circles). Experimental data in the unitary regime were excluded in the fit. These data points are to the left of the red solid line Fig. 3. Once the parameters of our approach are determined, we can use Eqs. (6) and (7) to predict the loss rate at a different temperature. Figure 3 shows also the resulting prediction for the loss rate at a temperature $4.5\,\mu{\rm K}$ (black dotted line) in comparison to the experimental data from Ref. [16] (black diamonds). Our results describe data at these small temperatures relatively well.

Note that the $B - B_0$ dependence of L_3 can be eliminated in favor of the $|a_1|$ dependence using Eq. (2). We have explicitly
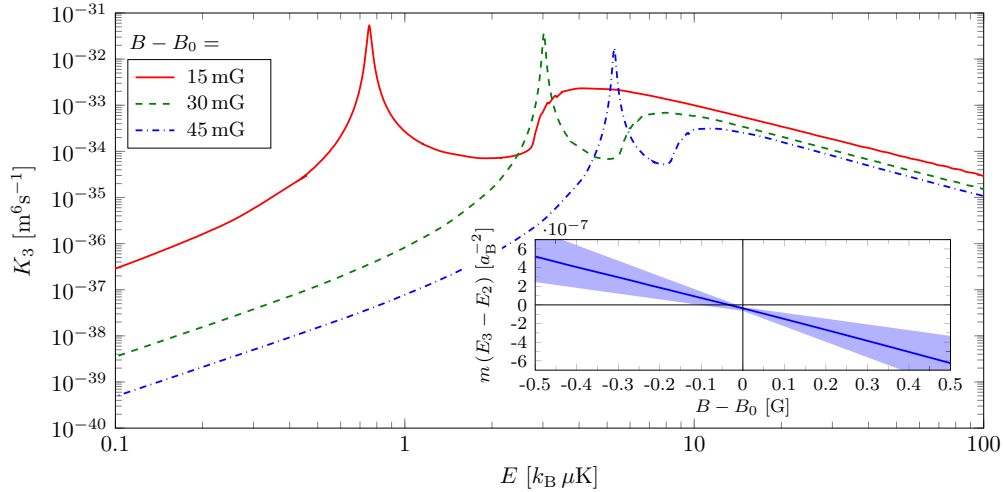
FIG. 4. Recombination rate K_3 as a function of the energy E for several field detunings $B - B_0$ at $\Lambda = 0.4 a_B^{-1}$. The inset shows the rescaled energy gap $m(E_3 - E_2)$ as a function of $B - B_0$ with an error estimate given by the shaded band.

checked that our loss rate results exhibit an $|a_1|^{8/3}$ scaling for small $|a_1| \lesssim 800/r_1^3$ as predicted by Suno *et al.* [33] and measured by Yoshida *et al.* [15].

The finite-temperature averaging of the energy-dependent recombination rate K_3 smears out the resonance features from the three-body loss rate. In Fig. 4, we show K_3 as a function of the energy for different magnetic field detunings. The curves have been generated with the parameters obtained in the fit to the $T = 2.1\,\mu$K data from Ref. [16] discussed above. They display a strong peak at lower energies followed by a sudden increase and a smooth fall off. The peak on the left is caused by the existence of a three-body resonance below the two-body resonance. Its position is controlled by the three-body force H. The sudden rise in K_3 to the right of the peak is the signature of the two-body resonance.

Given the fit results for r_1 and H, the difference of the three- and two-body resonance energies, $E_3 - E_2$, is a function of only the scattering volume, i.e., the magnetic field detuning. Thus, our approach allows us to predict the magnetic field dependence of the three-body resonance energy E_3. In the inset of Fig. 4, we show the rescaled energy gap $m(E_3 - E_2)$ as a blue line. For $B - B_0 > 0$, the three-body resonance is below the two-body resonance, and $E_3 - E_2$ is negative. Near $B - B_0 = 0$, E_3 is linear in B just like E_2, and the three-body resonance crosses the two-body energy. In the region $B - B_0 < 0$, the two-body resonance turns into a shallow bound state, and the energy difference $E_3 - E_2$ becomes positive.

Corrections to E_3 should arise from omitted J^P channels. Contributions of these channels to the loss rate $L_3(B)$ in the fit regime should have relative sizes $0 \leqslant \chi_3(B, T) \leqslant 1$ [see Eq. (18)]. Gaussian uncertainty propagation then implies a relative uncertainty of 46% for the χ^2 value of our fit. This number can be used as an estimate for the uncertainties of the offset α and slope β of the $m(E_3 - E_2) = \alpha + \beta(B - B_0)$ curve. We obtain $\alpha = -0.4(2) \times 10^{-7} a_B^{-2}$ and $\beta = -11(5) \times 10^{-7} a_B^{-2}/G$, which yield the blue band depicted in the inset of Fig. 4.

Let us emphasize that the three-body-state energy depends only on the resonance parameters a_1 and r_1 and the three-body

force H. In this sense, the state has some degree of universality. To our knowledge, there has not been direct experimental verification of this resonance so far. Such an experiment would be most helpful to assess our predictions and to gain a deeper understanding of universal binding mechanisms in the p-wave sector in general.

Finally, Fig. 5 shows the temperature-averaged loss rate L_3 as a function of the temperature T for different detunings $B - B_0$. The vertical lines denote the beginning of the unitary regime as given by Eq. (19), where the EFT power-counting approach is expected to fail. While the curves exhibit the expected T^{-2} behavior at large temperatures, they are not independent of B in the unitary regime. Instead, they are separated by factors of 1.3–1.5. We expect that effects from the unitary cut will be important in this region where the system is able to probe the resonance peak [29]. Moreover, the contribution from spin-parity channels different from $J^P = 1^+$ could be important. Even though suppressed close to $E = 0$, they might contribute significantly at finite temperature. It would also be instructive to iterate effects of the short-range three-body factor F. A nonperturbative treatment would presumably change the behavior at larger energies. Understanding the loss rate in this region is left to future work.

B. Comparison with Waseem *et al.*

We now compare our results to the two-body model employed by Waseem *et al.* [16] in the nonunitary regime,

$$K_3^{\text{Waseem}}(E) = \frac{144\sqrt{3}\pi^2}{m^3 E^2} \frac{\Gamma_e \Gamma_d}{(E - E_b)^2 + (\Gamma_e + \Gamma_d)^4/4},$$
(20)

where $\Gamma_e = -4\sqrt{m}E^{3/2}/r_1$, $\Gamma_d = -4/(mr_1a_1)$, and $E_b = k_{\text{res}}^2/m$ is the real part of the resonance energy.[3] While the temperature-averaged loss rate L_3 of Waseem *et al.* looks

---

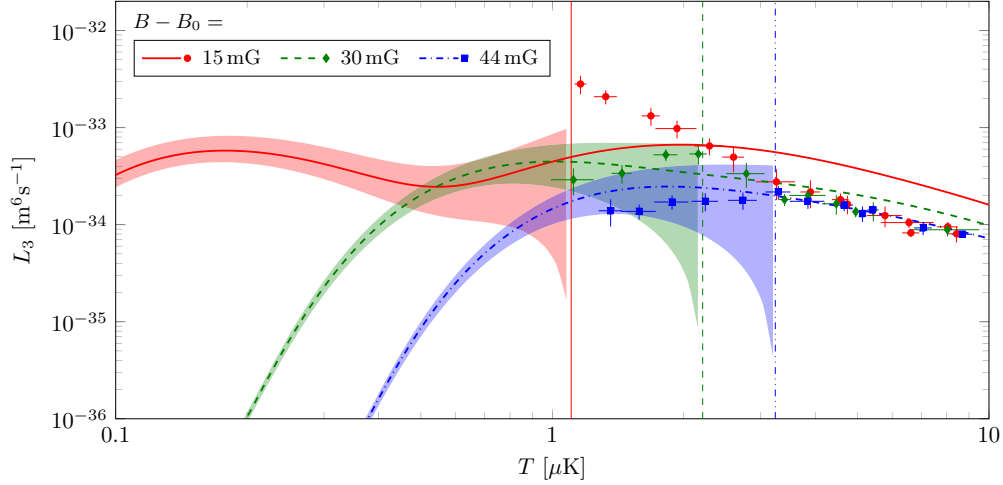[3]Note that we have converted Eq. (20) to our conventions with $\hbar = 1$.

FIG. 5. Loss rate L_3 as a function of the temperature T for several field detunings $B - B_0$ at $\Lambda = 0.4 a_B^{-1}$ (χ^2-fit predictions). Vertical grid lines at $p_T = k_{\mathrm{res}}$ separate the nonunitary (left) and unitary (right) regimes. Uncertainty bands are obtained as in Fig. 3.

similar to our result for the experimental temperatures, the energy-dependent recombination rate K_3 behaves very differently.

This can be seen in Fig. 6, where we compare the three-body recombination model in Eq. (20) and our results for a magnetic field detuning of $B - B_0 = 30$ mG. The inset shows that the temperature-averaged loss rates L_3 of both approaches agree for temperatures $T > 1\,\mu$K measured by Waseem *et al.* In contrast, the energy-dependent rate K_3 shows stark differences. The rate calculated in the EFT approach falls off at small energies as E^2, while the model in Eq. (20) grows as $E^{-1/2}$. Both approaches show a peak around $E = 3k_B\,\mu$K, but the microscopic origin is very different. In the model of Waseem *et al.* it is simply associated with the Breit-Wigner form put in by hand, while the resonance in the full three-body treatment in the EFT framework is dynamically generated

by the *p*-wave atom-atom interactions. Finally, there is a shoulder around $E = 7k_B\,\mu$K in the EFT framework which is not present in the model.

Currently, the data for the temperature-averaged loss rate are not able to distinguish between the two approaches and thus the underlying microphysics. The inset of Fig. 6, however, suggests that a new measurement at lower temperatures $T \lesssim 0.5\,\mu$K should be able to distinguish between the two scenarios.

Having outlined the differences in the nonunitary regime, we now compare the methods in the unitary regime. In this region, Waseem *et al.* use a T^{-2} ansatz with an adjustable coefficient and a functional form different from Eq. (20). They perform separate fits in the nonunitary and unitary regions, coinciding roughly at T_{unitary}. Results of these fits can be seen in the inset of Fig. 6 as solid and dotted
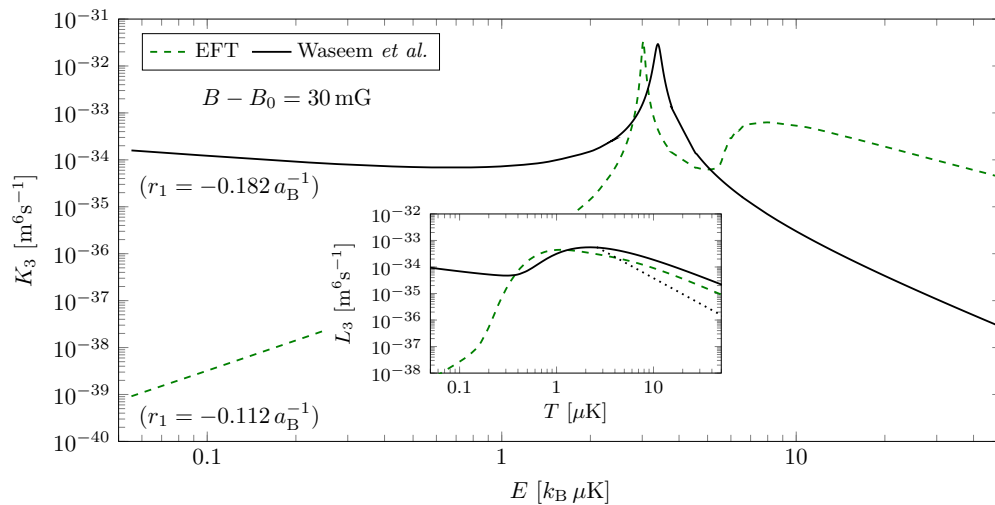

FIG. 6. Comparison of the energy-dependent recombination rate K_3 from our EFT calculation (dashed curve) and that from the model by Waseem *et al.* [16] (solid curve) as a function of the energy E for a magnetic-field detuning of $B - B_0 = 30$ mG. The inset shows the same comparison for the temperature-dependent loss rate L_3, where the dotted curve shows the T^{-2} behavior expected from unitarity. The dramatically different behaviors of the recombination rates at low energies lead to different predictions for the loss rates only at temperatures below $0.5\,\mu$K.

curves, respectively. This procedure leads to a good description of the temperature dependence in the unitary regime of Fig. 5.

Our leading-order EFT, in contrast, is adjusted in a single fit to the 2.1 μK data in Fig. 3, and all other curves are predictions. Moreover, it is solely designed to explain data in the nonunitary regime, where predictions are compatible with data within the uncertainty bands. In the unitary regime, the key assumption of dominance of the 1^+ partial wave is no longer satisfied, and our EFT breaks down. Thus, it is expected that we cannot describe the data above T_{unitary} in Fig. 5. In principle it is possible to formulate an EFT for the unitary regime by adding further partial-wave channels and so-far neglected two-body terms nonperturbatively. However, such an extension is beyond the scope of this work.

V. SUMMARY

In this work, we have considered the temperature-dependent three-body loss rate for a gas of identical fermions with resonant p-wave interactions. We have used an effective-field-theory approach to derive integral equations that describe the scattering of three fermions and used them to evaluate the rate for three-body recombination of polarized ^{6}Li atoms into deeply bound dimers and another atom. Our approach requires the determination of four parameters to become predictive: the scattering volume a_1, the effective range r_1, and two pieces of three-body information to determine the short-range three-body parameters H and F. The latter acts as an optical potential and parametrizes the coupling of the three-body system to final-state channels with deep dimers. We have used the known magnetic field dependence of the scattering volume a_1 and the experimental data from Waseem *et al.* [16] to fit the remaining parameters r_1, H, and F. Once these parameters are determined, we are also able to determine the position and magnetic field dependence of a fermionic three-body resonance with $J^P = 1^+$. This state exhibits some degree of universality in the sense of its energy position being dependent on only a_1 and r_1 and the three-body force H. We note that this three-body resonance could lead to interesting features in the three-body recombination rate on the positive-scattering-volume side of the Feshbach resonance, where the three-body state is a resonance close to the atom-dimer threshold. For positive scattering volume, it would also be interesting to consider atom-dimer relaxation as an additional benchmark to our approach.

While the temperature-averaged loss rates L_3 from the two-body resonance model employed in Ref. [16] and from our three-body calculation are very similar, the energy-dependent recombination rate $K_3(E)$ shows significant differences. New experiments at lower temperatures $T \leqslant 0.5$ μK should be able to distinguish between the two scenarios and determine the nature of the microscopic physics responsible for the loss processes.

In summary, we have shown that the three-body recombination rate $K_3(E)$ for spin-polarized ^{6}Li atoms with resonant p-wave interactions possesses interesting features due to two- and three-body resonances which can be seen at low temperatures. We also have demonstrated that three-body loss data can be used to extract detailed information on the two-body inter-

action once a reliable parametrization is established and used in a full three-body calculation. Our effective-field-theory approach has the additional advantage that the interaction is directly given in terms of the effective range parameters.

Waseem *et al.* recently described the unitary regime using a model for cascade processes that leads to a modified three-body loss rate L_3 [17]. Our uncertainty analysis led us to exclude this regime as more partial-wave channels are expected to contribute to the loss rate at these temperatures. It would therefore be interesting to include additional partial-wave channels in our calculation of the total loss rate in order to test their result and to analyze whether it is really necessary to include additional recombination mechanisms to achieve agreement with the data.

We finally note that the s-wave scattering between the $|F = 1/2, m_F = +1/2\rangle$ and $|F = 1/2, m_F = -1/2\rangle$ hyperfine states of ^{6}Li is moderately large (and negative) at the magnetic fields considered in this work [37]. The study of recombination losses in this two-component system of identical fermions with large s- and p-wave scattering lengths might therefore lead to interesting features such as a competition between odd- and even-parity recombination channels.

APPENDIX A: LAGRANGIAN

The EFT Lagrangian for the spin-polarized fermions can be split into three parts: $\mathcal{L} = \mathcal{L}_1 + \mathcal{L}_2 + \mathcal{L}_3$. For ^{6}Li atoms with mass $m = 6.0151223(5)$ u [38], the one-body part

$$\mathcal{L}_1 = \psi^\dagger \left[i\partial_0 + \frac{\nabla^2}{2m} \right] \psi \tag{A1}$$

can be written in terms of scalar fields ψ, $\psi^\dagger$ which anticommute.

The remaining parts comprise all two- and three-body contact terms compliant with Galilean symmetry. They are formulated using bosonic fields π_{m_l}, $\pi_{m_l}^\dagger$ ($m_l \in \{-1, 0, 1\}$), which annihilate and create two atoms in a p wave, respectively. At LO, $\mathcal{L}_2$ reads

$$\mathcal{L}_2 = \pi_{m_l}^\dagger \left[\Delta + \left(i\partial_0 + \frac{\nabla^2}{4m} \right) + \cdots \right] \pi_{m_l}$$
$$- \frac{g}{\sqrt{2}} \left[\pi_{m_l}^\dagger \left(\psi \{ -i \overleftrightarrow{\nabla}_2 \}_{1m_l} \psi \right) + \text{H.c.} \right], \tag{A2}$$

where H.c. is the Hermitian conjugate and the sums over m_l are implicit. The p-wave nature of the diatom manifests itself in the tensor structure $\{\cdot\}_{1m_l}$. Together with the Galilean-invariant derivative $\overleftrightarrow{\nabla}_2 \equiv (\overleftarrow{\nabla} - \overrightarrow{\nabla})/2$, it contributes a factor

$$\{\boldsymbol{k}\}_{1m_l} \equiv (4\pi/3)^{1/2} \, k \, Y_1^{m_l}(\hat{\boldsymbol{k}}) \tag{A3}$$

to the π-$\psi\psi$ vertex. Here, $\boldsymbol{k} = (\boldsymbol{k}_1 - \boldsymbol{k}_2)/2$ is the atom-atom relative momentum. To describe a shallow p-wave resonance, two real low-energy parameters are required [29,39]. They are chosen as Δ and the coupling g, both of which will be matched to observables.

The three-body part $\mathcal{L}_3$ contains three-body interactions which eliminate potential divergences in different spin-parity channels J^P. At LO, a single three-body force ($J^P = 1^+$)

enters the theory. It takes the form

$$\mathcal{L}_3 = -C_0^{(1^+)} \frac{12\pi}{mg^2} (\psi \, \boldsymbol{\pi})_{m_J}^{(1^+)\,\dagger} (\psi \, \boldsymbol{\pi})_{m_J}^{(1^+)} + \cdots \tag{A4}$$

with the $J^P = 1^+$ ($l = L = J = 1$) field combinations

$$(\psi \, \boldsymbol{\pi})_{m_J}^{(1^+)} = \sqrt{3} \, C_{1m_L, 1m_l}^{1m_J} \psi \{-i \overleftrightarrow{\nabla}_3\}_{1m_L} \pi_{m_l} \tag{A5}$$

and the Galilean-invariant derivative $\overleftrightarrow{\nabla}_3 \equiv (2\overleftarrow{\nabla} - \overrightarrow{\nabla})/3$. Further, we define a dimensionless three-body force $H^{(1^+)}$ with

$$C_0^{(1^+)}(\Lambda) = H^{(1^+)}(\Lambda)/\Lambda^2. \tag{A6}$$

APPENDIX B: FADDEEV EQUATION

The Feynman rules resulting from the Lagrangian given in the previous section can be used to derive an integral equation for atom-dimer scattering. For orbital angular momentum quantum numbers $l = l' = 1$ and projections m_l and $m_{l'}$, this Faddeev integral equation is given by

$$T^{m_l, m_l'}(\boldsymbol{p}, \boldsymbol{p}'; p_E) = -V^{m_l, m_l'}(\boldsymbol{p}, \boldsymbol{p}'; p_E) + \sum_{m_l''} \int \frac{d^3q}{(2\pi)^3} V^{m_l, m_l''}(\boldsymbol{p}, \boldsymbol{q}; p_E) G_\pi(\tilde{k}(q^2)) T^{m_l'', m_l'}(\boldsymbol{q}, \boldsymbol{p}'; p_E), \tag{B1}$$

where $\tilde{k}(q^2)$ is given in Eq. (9). The particle exchange potential is given by

$$-iV^{m_l, m_l'}(\boldsymbol{p}, \boldsymbol{q}; p_E) = -i24\pi \frac{\{\boldsymbol{q} + \boldsymbol{p}/2\}_{1m_l}^* \{\boldsymbol{p} + \boldsymbol{q}/2\}_{1m_l'}}{p^2 + q^2 - p_E^2 + \boldsymbol{p} \cdot \boldsymbol{q}} \tag{B2a}$$

$$= -i \sum_J \sum_{L, L'} V^{^3L_J, ^3L_J'}(p, q; p_E) 4\pi \sum_{m_J} [\boldsymbol{Y}_{(L,1)Jm_J}(\hat{\boldsymbol{p}})]^{m_l} [\boldsymbol{Y}_{(L',1)Jm_J}(\hat{\boldsymbol{q}})]^{m_l'\,*}. \tag{B2b}$$

Projection onto partial waves with $l = 1$, total orbital angular momentum L, and total angular momentum J yields

$$V^{^3L_J, ^3L_J'}(p, q; p_E) = -24\pi \frac{\sqrt{(2L+1)(2L'+1)}}{2J+1} \left[C_{L0,10}^{J0} C_{L'0,10}^{J0} \frac{1}{2} \left(\frac{p}{q} \hat{t}_{L'} + \frac{q}{p} \hat{t}_L \right) \right.$$

$$\left. + pq \left(\frac{1}{4} C_{L0,10}^{J0} C_{L'0,10}^{J0} \hat{t}_J + (2J+1) \sum_k C_{L0,10}^{k0} C_{L'0,10}^{k0} \begin{Bmatrix} 1 & J & L' \\ 1 & k & L \end{Bmatrix} \hat{t}_k \right) \right] Q_. \left(\frac{p_E^2 - p^2 - q^2}{pq} \right), \tag{B3}$$

where $Q_.$ are Legendre functions of the second kind in the convention of Ref. [35] and the short notation $\hat{t}_L Q_. \equiv Q_L$ was used. For the 1^+ channel ($l = L = J = 1$), we recover Eq. (11).

[1] E. Braaten and H.-W. Hammer, Phys. Rep. **428**, 259 (2006).

[2] S. Giorgini, L. P. Pitaevskii, and S. Stringari, Rev. Mod. Phys. **80**, 1215 (2008).

[3] C. Chin, R. Grimm, P. Julienne, and E. Tiesinga, Rev. Mod. Phys. **82**, 1225 (2010).

[4] P. Naidon and S. Endo, Rep. Prog. Phys. **80**, 056001 (2017).

[5] C. H. Greene, P. Giannakeas, and J. Pérez-Ríos, Rev. Mod. Phys. **89**, 035006 (2017).

[6] V. Efimov, Phys. Lett. B **33**, 563 (1970).

[7] E. Nielsen and J. H. Macek, Phys. Rev. Lett. **83**, 1566 (1999).

[8] B. D. Esry, C. H. Greene, and J. P. Burke, Phys. Rev. Lett. **83**, 1751 (1999).

[9] P. F. Bedaque, E. Braaten, and H.-W. Hammer, Phys. Rev. Lett. **85**, 908 (2000).

[10] E. Braaten and H.-W. Hammer, Phys. Rev. Lett. **87**, 160407 (2001).

[11] T. Kraemer, M. Mark, P. Waldburger, J. G. Danzl, C. Chin, B. Engeser, A. D. Lange, K. Pilch, A. Jaakkola, H.-C. Naegerl *et al.*, Nature (London) **440**, 315 (2006).

[12] J. Zhang, E. G. M. van Kempen, T. Bourdel, L. Khaykovich, J. Cubizolles, F. Chevy, M. Teichmann, L. Tarruell, S. J. J. M. F. Kokkelmans, and C. Salomon, Phys. Rev. A **70**, 030702(R) (2004).

[13] C. H. Schunck, M. W. Zwierlein, C. A. Stan, S. M. F. Raupach, W. Ketterle, A. Simoni, E. Tiesinga, C. J. Williams, and P. S. Julienne, Phys. Rev. A **71**, 045601 (2005).

[14] C. A. Regal, C. Ticknor, J. L. Bohn, and D. S. Jin, Phys. Rev. Lett. **90**, 053201 (2003).

[15] J. Yoshida, T. Saito, M. Waseem, K. Hattori, and T. Mukaiyama, Phys. Rev. Lett. **120**, 133401 (2018).

[16] M. Waseem, J. Yoshida, T. Saito, and T. Mukaiyama, Phys. Rev. A **98**, 020702(R) (2018).

[17] M. Waseem, J. Yoshida, T. Saito, and T. Mukaiyama, Phys. Rev. A **99**, 052704 (2019).

[18] M. Jona-Lasinio, L. Pricoupenko, and Y. Castin, Phys. Rev. A **77**, 043611 (2008).

[19] Y. Nishida, Phys. Rev. A **86**, 012710 (2012).

[20] E. Braaten, P. Hagen, H.-W. Hammer, and L. Platter, Phys. Rev. A **86**, 012711 (2012).

[21] H.-W. Hammer and L. Platter, Annu. Rev. Nucl. Part. Sci. **60**, 207 (2010).

[22] H.-W. Hammer, S. König, and U. van Kolck, arXiv:1906.12122.

[23] B. R. Levy and J. B. Keller, J. Math. Phys. **4**, 54 (1963).

[24] B. Gao, Phys. Rev. A **58**, 4222 (1998).

[25] P. Zhang, P. Naidon, and M. Ueda, Phys. Rev. A **82**, 062712 (2010).

[26] T. Nakasuji, J. Yoshida, and T. Mukaiyama, Phys. Rev. A **88**, 012710 (2013).

[27] J. Levinsen, N. R. Cooper, and V. Gurarie, Phys. Rev. A **78**, 063616 (2008).

[28] G. M. Bruun, A. D. Jackson, and E. E. Kolomeitsev, Phys. Rev. A **71**, 052713 (2005).

[29] P. F. Bedaque, H.-W. Hammer, and U. van Kolck, Phys. Lett. B **569**, 159 (2003).

[30] M. Schmidt, Ph.D. thesis, Technische Universität Darmstadt, 2019, http://tuprints.ulb.tu-darmstadt.de/8778/.

[31] E. Braaten and H.-W. Hammer, Phys. Rev. A **70**, 042706 (2004).

[32] B. D. Esry, C. H. Greene, and H. Suno, Phys. Rev. A **65**, 010705(R) (2001).

[33] H. Suno, B. D. Esry, and C. H. Greene, Phys. Rev. Lett. **90**, 053202 (2003).

[34] J. P. D'Incao, H. Suno, and B. D. Esry, Phys. Rev. Lett. **93**, 123201 (2004).

[35] M. Abramowitz and I. A. Stegun, *Handbook of Mathematical Functions* (Dover, New York, 1964).

[36] H. Suno, B. D. Esry, and C. H. Greene, New J. Phys. **5**, 53 (2003).

[37] P. S. Julienne and J. M. Hutson, Phys. Rev. A **89**, 052715 (2014).

[38] J. R. de Laeter, J. K. Böhlke, P. De Bièvre, H. Hidaka, H. S. Peiser, K. J. R. Rosman, and P. D. P. Taylor, Pure Appl. Chem. **75**, 683 (2003).

[39] C. A. Bertulani, H.-W. Hammer, and U. Van Kolck, Nucl. Phys. A **712**, 37 (2002).